

Real-Time and Continuous Monitoring of Brain Deformation

Ziwei Liu, Chengqiang Tang, Jianzheng Li, Yiqing Yang, Wenjun Li, Jiajia Wang, Sihui Yu, Chuang Wang, Yajie Qin, Qi Tong, Xuemei Sun,* and Huisheng Peng*

Researchers have typically studied the brain by monitoring characteristic signals, such as electrophysiology and neurotransmitters by implanted electronics. Here, real-time monitoring of dynamic deformations of the brain tissue *in vivo*, is demonstrated, as a new characteristic parameter that is reflective of brain states. As a proof of concept, a thin capacitive deformation sensor is fabricated and implanted between the skull and cortex, and the sensor is shown to effectively monitor dynamic deformations of the cortical surface in the rat brain as induced by respiration and heartbeat under different degrees of anesthesia. This brain monitoring approach based on deformation signals opens up a new direction for understanding the brain.

deconstruction of neural circuits in the combination of optics and genetics.^[6] Such monitoring of intrinsic properties of the brain plays a decisive role in advancing our understanding of the brain, but there is still a lack of systematic research considering mechanical signals, such as the real-time dynamic deformations. The dynamic deformation is a direct indicator to reveal the mechanical and structural properties of the brain tissue, and the brain deformation is also used in the clinical diagnosis of traumatic brain injury^[7] and tumor growth.^[8]

Brain tissue is constantly undergoing dynamic deformations similar to the

1. Introduction

Studying the brain is a crucial and enduring topic. A range of monitoring methods have been developed to gain insight into the highly integrated brain network. In 1791, the electrical properties of neurophysiology were reported,^[1] and electrophysiological signals, including local field potentials and action potentials were recorded by using implanted neural electrodes to decode the brain.^[2] In the 1970s, chemicals in the brain were measured through implanted electrochemical sensors,^[3] which enabled the analysis of neurotransmitter distribution and change.^[4] In the early 2000s, optogenetics flourished^[5] and enabled the precise


heart, e.g., microvascular blood volume pulsations are generated by respiration and heartbeat under a normal physiological state, which lead to tiny brain deformations.^[9] Such deformations will cause relative micromotions between neural devices and brain tissues, which is considered one of the main challenges inhibiting chronic brain recording.^[10] Additionally, a certain degree of brain deformation has been reported to be related to developmental processes^[11] and diseases, such as epilepsy^[12] and brain tumors.^[13] Even the vasodilation of cerebral vessels induced by isoflurane could change brain deformation.^[14] Therefore, monitoring dynamic deformations of the brain tissue will provide a novel methodology for studying the brain. However, the reliable monitoring of brain deformation in animals under different activity states requires sufficient temporal resolution, continuity and wearability, which cannot be achieved by existing imaging methods, such as X-ray and magnetic resonance imaging (Table S1, Supporting Information). As a result, this intrinsic property of the brain is underdeveloped, resulting in a “missing piece” in the puzzle of brain science.

Here, we report real-time monitoring of brain deformation as a new direction for neuroscience. To this end, an implanted brain deformation sensor (BDS) was developed. Based on the principle of capacitive sensing, real-time and highly sensitive monitoring of deformation was realized. The BDS consisted of two ultrathin ($\approx 2 \mu\text{m}$) and low-density ($\approx 1.23 \text{ g cm}^{-3}$) electrodes, where one was adhered to the cortex and the other was fixed on the skull (Figure 1a). Deformation of brain tissue changed the distance between the two electrodes, leading to the varied capacitance (Figure 1b). Through the utilization of BDS, brain deformations induced by respiration and heartbeat were monitored and dissociated, and the relationship between the anesthetic depth and the brain deformation was revealed. This brain deformation monitoring provides a new and attractive methodology for multidimensional study of the brain.

Z. Liu, C. Tang, Y. Yang, W. Li, J. Wang, S. Yu, C. Wang, X. Sun, H. Peng
State Key Laboratory of Molecular Engineering of Polymers
Department of Macromolecular Science
Institute of Fiber Materials and Devices
and Laboratory of Advanced Materials
Fudan University
Shanghai 200438, China
E-mail: sunxm@fudan.edu.cn; penghs@fudan.edu.cn

J. Li, Y. Qin
School of Information Science and Technology
Fudan University
Shanghai 200438, China

Q. Tong
Department of Aeronautics and Astronautics
Fudan University
Shanghai 200433, China

 The ORCID identification number(s) for the author(s) of this article can be found under <https://doi.org/10.1002/aelm.202300732>

© 2024 The Authors. Advanced Electronic Materials published by Wiley-VCH GmbH. This is an open access article under the terms of the [Creative Commons Attribution](https://creativecommons.org/licenses/by/4.0/) License, which permits use, distribution and reproduction in any medium, provided the original work is properly cited.

DOI: 10.1002/aelm.202300732

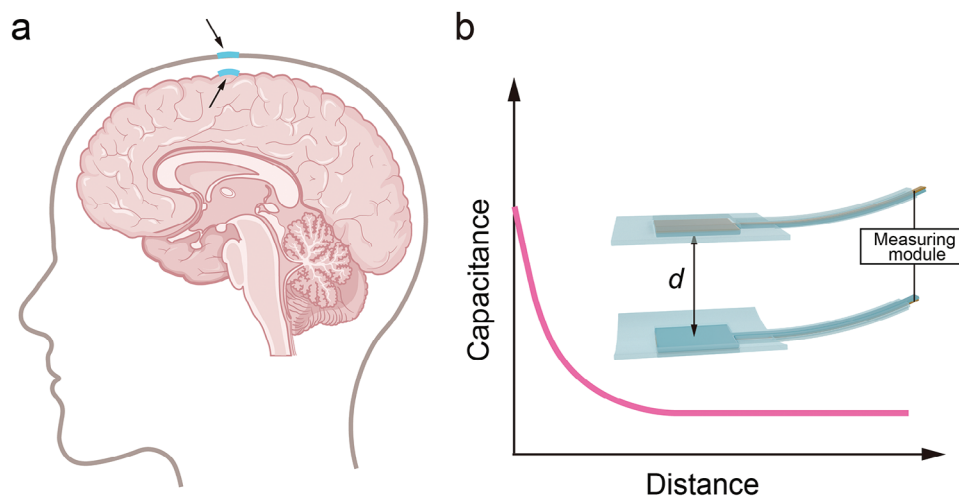


Figure 1. Concept and design for monitoring brain deformation. a) Illustration of a brain deformation sensor (BDS) consisting of two thin film electrodes attached on the skull and cortex. The black arrows indicated the electrodes. b) Schematic of the deformation monitoring system (inset) and its capacitive sensing principle.

2. Results and Discussion

The BDS was designed to be lightweight and thin to avoid affecting the dynamic deformations of brain tissue after implantation and to guarantee reality. The electrode was constructed as a sandwich structure where polydimethylsiloxane (PDMS) was used as the substrate and gold (Au) was used as the conductive layer between PDMS substrates. Through micro- and nanofabrication, mass preparation of BDS was realized (Figure 2a). The substrate had dimensions of 4 mm × 4 mm with Au electrode area of 2 mm × 2 mm in the center, and the total thickness of the electrode was ≈2 μm (Figure 2b,c). The electrodes of BDS maintained stable conductivity within ≈20% strain and cyclic bending (Figure S1, Supporting Information), which performed a certain reliability in capacitive monitoring. A layer of polydopamine (PDA) with a thickness of ≈100 nm was formed on the surface of PDMS by oxidative polymerization (Figures S2 and S3, Supporting Information).^[15] PDA helped firmly attach to the brain tissue, allowing the electrode and the tissue to move together (Figure 2d). To evaluate adhesion, the bare PDMS film and PDA-modified PDMS film were attached to the brain surface and then separated by a tension machine. The results showed that the PDA-modified PDMS film exhibited a peak force six times that of the unmodified PDMS, which could even accommodate the weight of the rat brain (Figure 2e). This allowed the electrode to contact stably with the brain tissue during dynamics without suture and to follow rapid deformations without retardation. The density of the electrode was ≈1.23 g cm⁻³, close to that of brain tissue (1.04 g cm⁻³)^[16] and typically used implanted flexible materials (e.g., polyimide, 1.40 g cm⁻³)^[17] (Figure 2f). The approximate density rendered the electrode not to cause significant compression and collapse to the brain tissue, which was proven by the finite element analysis (Figure 2g). Additionally, there was no significant compression or damage to the coronal sections after implantation of BDS for 2 weeks (Figure 2h).

To prove that BDS could respond to rapid deformations, such as brain tissue, a series of simulative experiments were performed in vitro. The BDS was connected to the printed circuit board for capacitance detection using a two-channel flexible printed circuit (Figure S5, Supporting Information). As shown in Figure 3a, the capacitance of BDS changed by ≈800 fF within 1.0 mm. Furthermore, the sensitivity (S) of BDS could be defined as $S = \Delta C / \Delta d$, where ΔC and Δd indicate the changes in capacitance and distance, respectively. The sensitivity of BDS was more than 22.4 fF μm⁻¹ when the distance was <500 μm (Figure 3b). And in a certain range of temperature and humidity, capacitance monitoring was not greatly influenced (Figure S6, Supporting Information). In addition, the distance of 500 μm between the electrodes was controlled to change programmatically at speeds between 60 and 10 mm min⁻¹, and the capacitance steadily matched with the distance variation (Figure 3c). The responses of BDS under vibration at different frequencies were also measured. Agarose gel (0.6 wt%) mimicked brain tissue and was fixed on a plate that could vibrate at a determined frequency. The bottom electrode of BDS was adhered to the agarose gel, and the top electrode was fixed directly above the bottom electrode for capacitance monitoring (Figure 3d). In the range of 1–10 Hz, BDS could accurately follow the movement of agarose gel, and the capacitance variation corresponded with the reciprocating vibration cycles (Figure 3e). These results proved that BDS had excellent tracking ability for high-frequency motion without detachment from the designated location. To further simulate the expansion and contraction of the brain tissue, the balloon, agarose gel, and acrylic spherical mold were assembled to simulate intracranial blood volume, the brain tissue and the skull, respectively (Figure 3f). Two electrodes of BDS were attached on agarose gel and an acrylic spherical mold. The volume was controlled through the inflation and deflation of the syringe to simulate brain dynamics, while BDS could monitor the deformation of the top surface of the agarose gel. The controlled frequency and amplitude changes of the agarose gel were accurately

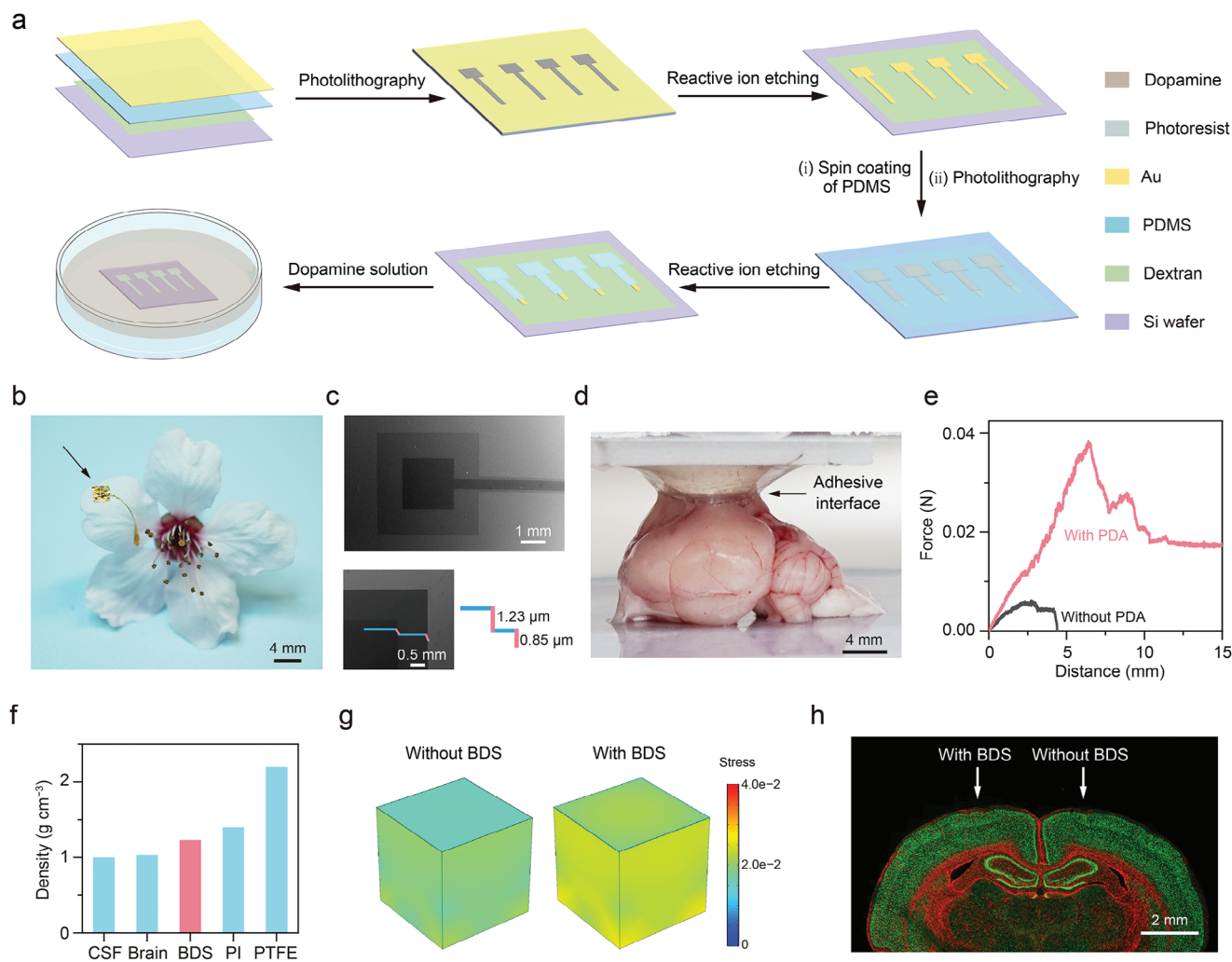


Figure 2. Preparation and morphology of BDS. a) Schematics of the preparation process of BDS, including thermal evaporation, photolithography, reactive ion etching, and polydopamine modification in sequence, followed by peeling off the silicon wafer. b) Photograph of a BDS placed on a cherry blossom petal. c) Typical SEM images of the BDS (without PDA), with an overall thickness of $\approx 2 \mu\text{m}$. The top PDMS layer was $0.85 \mu\text{m}$, and the total thickness of the Au and bottom PDMS layers was $1.23 \mu\text{m}$. d) Photograph of the interface between the PDA-modified PDMS film and the rat brain. The PDMS film was fixed on a hollow foam frame with the modified side in contact with the rat brain, and then lifted by a tensile machine. e) The forces during the separation process between the rat brain and PDMS films with/without PDA. f) Density comparison of BDS with brain substances and typical biomedical materials. CSF: cerebrospinal fluid, 1.00 g cm^{-3} ; brain: 1.04 g cm^{-3} ; [16] BDS: 1.23 g cm^{-3} ; PI: polyimide, 1.40 g cm^{-3} ; [17] PTFE: polytetrafluoroethylene, 2.20 g cm^{-3} . [18] g) Mechanical simulation of the brain surface with/without BDS. The size of the brain tissue model was $2 \text{ mm} \times 2 \text{ mm} \times 2 \text{ mm}$ and the size of the BDS electrode was $2 \text{ mm} \times 2 \text{ mm} \times 2 \mu\text{m}$. The brain tissue without BDS was covered with CSF. They were in contact with each other, and the electrode or equivalent CSF was subjected to downward gravity. Models were shown in Figure S4 (Supporting Information). h) Fluorescence image of the coronal section of rat brain taken after implanting BDS for 2 weeks, showing negligible immune responses.

reflected in the capacitance curves of BDS (Figure 3g). Increasing the flow rate led to a higher frequency of capacitance change, while the larger flow resulted in a greater amplitude change, as expected.

The BDS was subsequently integrated into a wireless and lightweight signal acquisition system and implanted into the rat brain. The system could perform real-time tracking of rat brain deformation (Figure 4a,b). The PDA-modified electrode was closely attached to the brain tissue of the rat, ensuring a consistent baseline during monitoring (Figure S7, Supporting Information). The immunohistochemical analysis of coronal sections

showed good biocompatibility of BDS after implantation, and no clear injury or collapse was observed (Figure S8, Supporting Information).

Brain deformation monitoring was demonstrated through an anesthetic model in rats. The isoflurane concentration was chosen as the quantitative control parameter of anesthesia in rats, which realized a simple state paradigm to generate switches of spontaneous brain deformations. The isoflurane concentration was adjusted to 1.0%, 1.5%, and 2.0% ($V_{\text{isoflurane}}:V_{\text{air}}$). The deformation curves were recorded by BDS after reaching a stable state, as shown in Figure 4c. Every curve had characteristic spikes

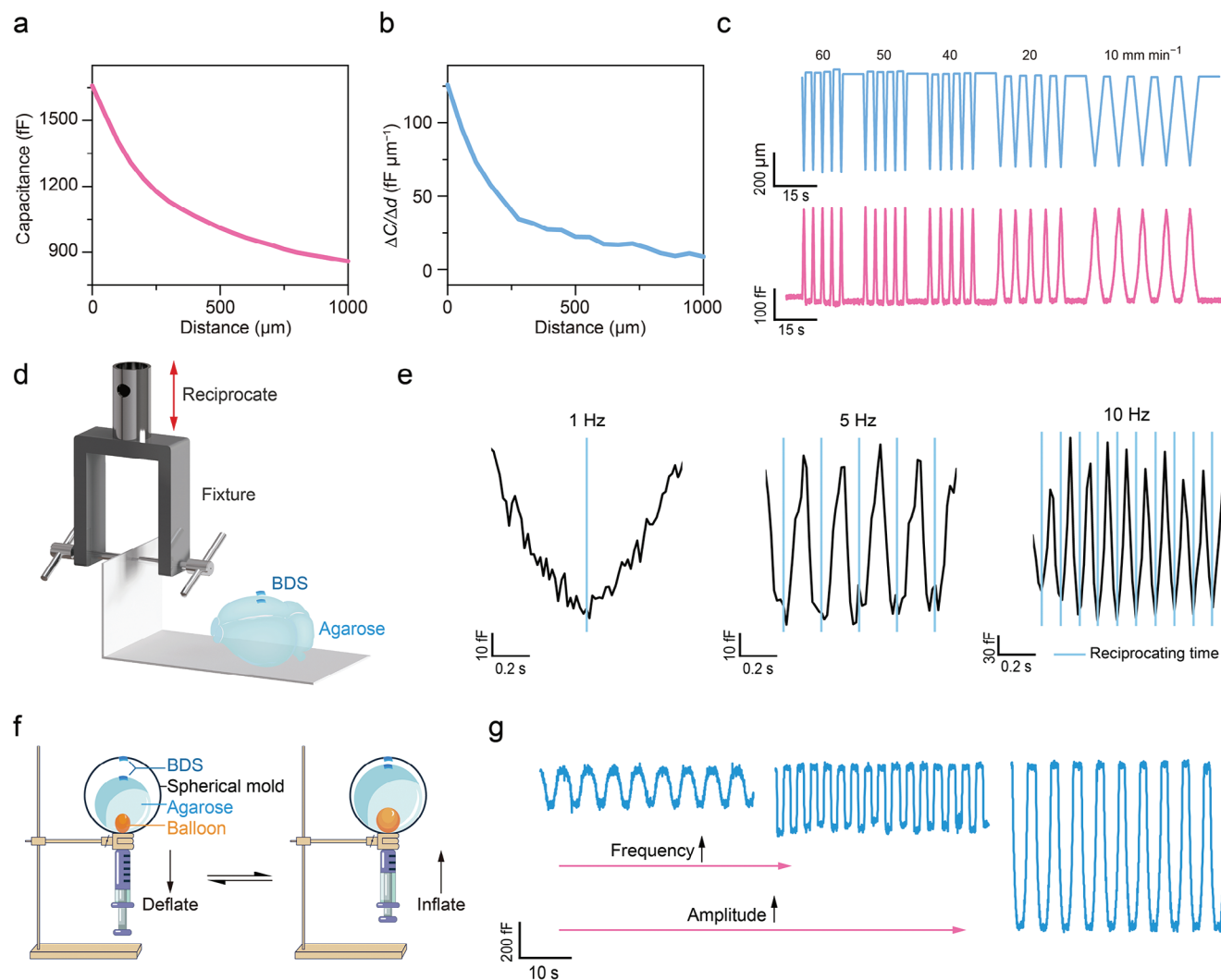


Figure 3. Sensing performances of BDS. a) Capacitive response of BDS to increasing distance between two electrodes. b) Response of $\Delta C/\Delta d$ to the distance between two electrodes, where ΔC is the capacitance change, and Δd is the distance change. $\Delta C/\Delta d$ is the capacitance change with distance, which was $>22.4 \text{ fF } \mu\text{m}^{-1}$ when the distance was $<500 \mu\text{m}$. c) Response of BDS for repeated distance changes of $500 \mu\text{m}$ at different speeds. d) Schematic illustration of the equipment for vibration monitoring. The agarose attached to BDS was driven to reciprocate at certain frequencies (similar to the vibration), and the motion was monitored by BDS. e) The capacitances were monitored under different frequencies of vibration, which well matched the given frequency. f) Schematic illustration of the equipment for monitoring of simulating brain deformations by using a balloon, agarose, and acrylic spherical mold. The balloon was connected to a syringe. The volume of the agarose was changed by inflating and deflating the balloon through a syringe. g) Capacitive responses of BDS to the inflation and deflation of the balloon under different frequencies and amplitudes in (f).

and valleys (Figure 4d), representing the effects of heartbeat and respiration on brain deformation in terms of frequency, which was consistent with the electrocardiograph and end-tidal carbon dioxide wave (Figure S9, Supporting Information). To eliminate the effects of electrical disturbances or noise resulting from the rat's respiratory activity, the bottom electrode of BDS was adhered to the rat skull, and the top electrode was fixed directly above the bottom electrode for capacitance monitoring. The capacitance curve exhibited no discernible respiratory or heartbeat components, which proved that the signals measured as the BDS electrodes were placed on the cortex and skull, respectively, were genuine brain deformation signals (Figure S10, Supporting Information). The brain deformation signals were then decoupled

to obtain specific deformation signals induced by respiration and heartbeat through data analysis based on frequency and amplitude differences (Figure 4e,f; Figure S11, Supporting Information). Subsequently, a statistical analysis was performed on the deformation signals ($n = 10$). The amplitude ratio was used for analysis, which was defined as the proportion of the deformation amplitude caused by respiration or heartbeat to the total deformation amplitude. With the deepening of anesthesia from 1.0% to 2.0%, the amplitude ratio of brain deformation induced by respiration decreased from $76.1 \pm 14.5\%$ to $47.1 \pm 12.4\%$. In contrast, the amplitude ratio induced by heartbeat gradually increased from $23.9 \pm 14.5\%$ to $52.9 \pm 12.4\%$ (Figure 4g,h). This observed change was attributed to the increase in isoflurane

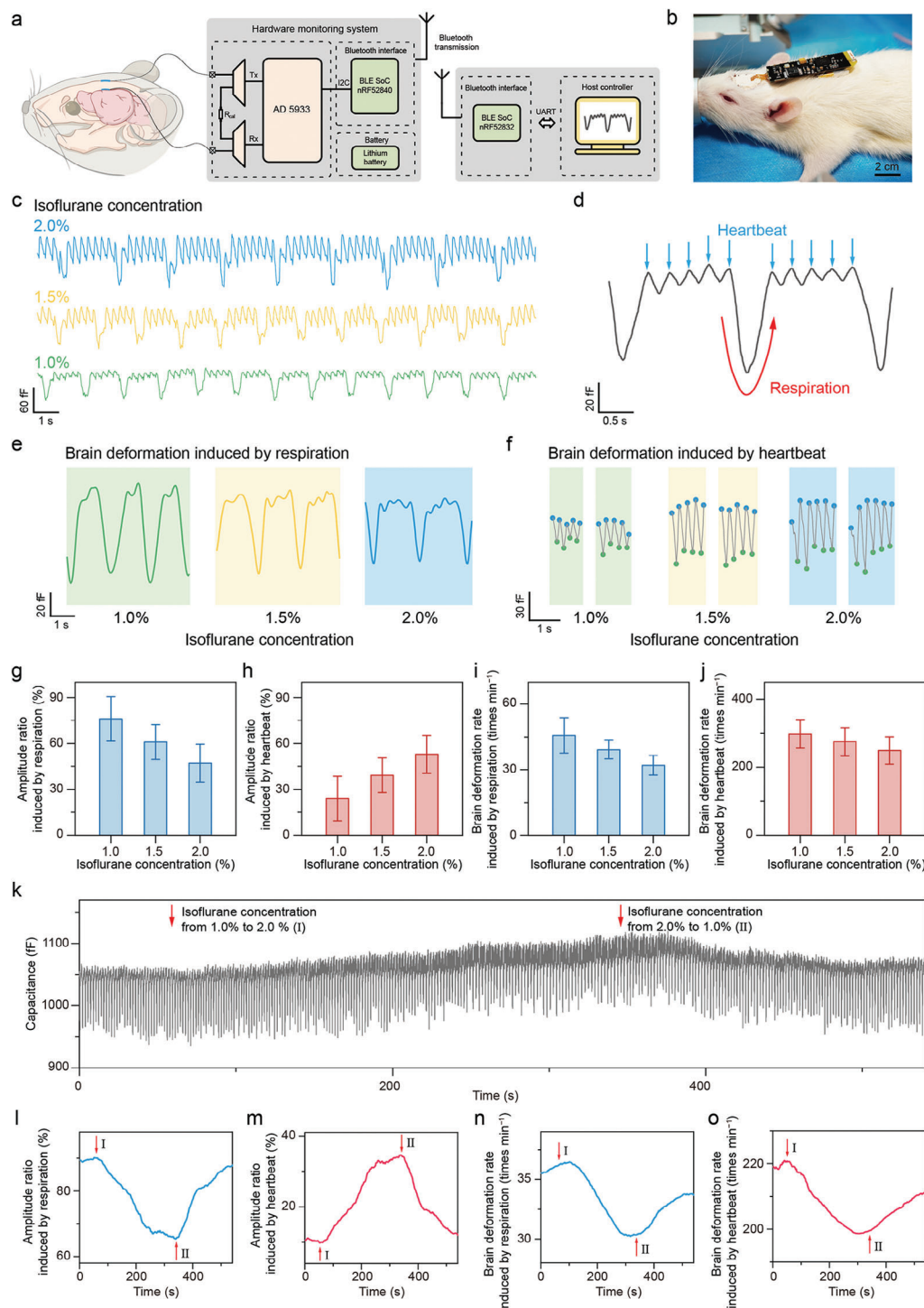


Figure 4. Real-time and continuous monitoring of brain deformation in vivo. a) Construction of the brain deformation monitoring system composed of BDS and measuring module. The brain deformation signals were monitored through a hardware monitoring system, and then transferred to a host computer via Bluetooth. b) Photograph of the system utilized in rat brain. c) Capacitance curves reflecting the rat brain deformations monitored at 1.0%, 1.5%, and 2.0% isoflurane concentrations ($V_{\text{isoflurane}} \cdot V_{\text{air}}$) after the rat reached steady anesthesia. d) Zoomed-in curve in (c) containing respiratory and heartbeat signals. The red and blue arrows represented the brain deformations induced by respiration and heartbeat, respectively. e, f) Fragments of capacitance curves reflecting the rat brain deformations induced by respiration (e) and heartbeat (f) through algorithmic decoupling at different isoflurane concentrations. g, h) Statistical plots of the amplitude ratio induced by respiration (g) and heartbeat (h) to the overall brain deformations at different isoflurane concentrations ($n = 10$, mean \pm s.d.). i, j) Statistical plots of the brain deformation rate induced by respiration (i) and heartbeat (j) at different isoflurane concentrations ($n = 10$, mean \pm s.d.). k) Real-time and continuous monitoring of rat brain deformations during the change in isoflurane concentrations from 1.0% to 2.0% (I) and then to 1.0% (II). l, m) Analysis of brain deformation amplitude variation trends induced by respiration (l) and heartbeat (m) in (k). n, o) Analysis of the brain deformation rate changes induced by respiration (n) and heartbeat (o) in (k).

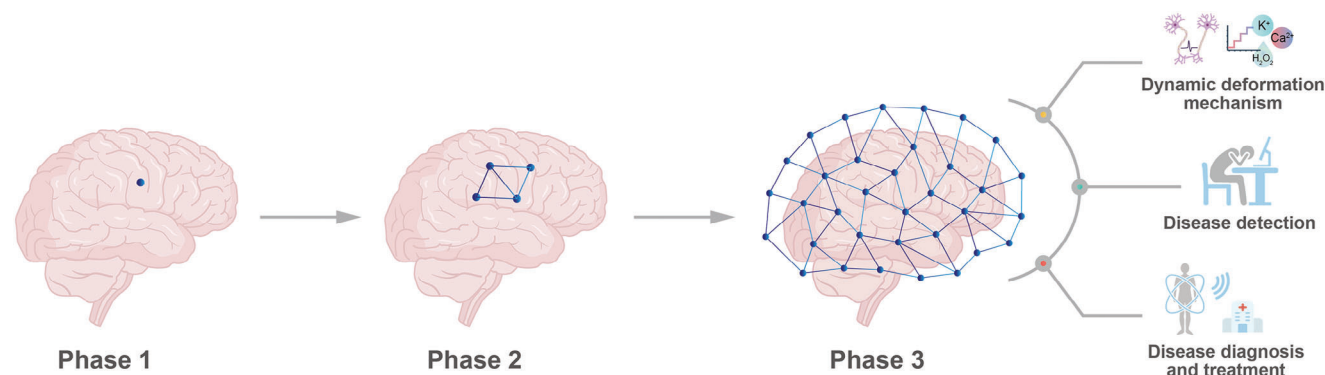


Figure 5. Schematic of brain deformation mapping and promising applications.

concentration, which induced the hypoxic state of rats.^[19] Additionally, the brain deformation rate (the brain deformation times per minute) generated by respiration or heartbeat decreased as anesthesia deepened, showing inhibited brain dynamics (Figure 4i,j). This was attributed to the effect of anesthetics on the central nervous system, which inhibited the conduction of neural signals, leading to a reduction in respiratory and heartbeat rates.^[19,20]

The reliable monitoring system was subsequently applied in real-time and continuous monitoring of brain deformation during anesthesia state switches. The isoflurane concentration was increased from 1.0% to 2.0% at 60 s (I) and decreased from 2.0% to 1.0% at 340 s (II), and the real-time deformations of the brain were shown with a similar variation pattern as above (Figure 4k–o). After changing the isoflurane concentration for ≈ 200 s, the deformations induced by respiration and heartbeat gradually became invariant, revealing that the rats reached a stable physiological state. Notably, as the anesthesia state changed (I and II), the brain deformation responded immediately (I and II in Figure 4l–o). Therefore, the monitoring of brain deformation revealed how this deformation is influenced by respiration and heartbeat. In addition, the baseline in Figure 4k showed an escalating trend with the deepening of the anesthesia because isoflurane increased cerebral blood flow and induced vasodilation, enlarging the brain volume.^[21] With BDS, continuous real-time monitoring of brain deformations becomes possible, and transient brain deformations due to incidental head impacts in living animals can also be detected (Figure S12, Supporting Information), which provides a methodology for studying the brain, such as intrinsic mechanical properties of brain tissue including viscoelasticity and traumatic brain injury. This information is difficult to obtain by imaging methods such as magnetic resonance imaging.

3. Conclusion

In summary, we successfully achieved real-time and continuous monitoring of brain deformation through a capacitive sensor. As a proof of concept, we presented the dynamic brain deformations of the rat under different anesthetic depths with an implanted sensor. Moreover, dynamic brain deformations induced by respiration and heartbeat were clearly distinguished. Thus, we have taken the first step in monitoring dynamic brain deformations in

vivo and presented a new avenue for exploring the brain. In the future, our sensor will be extended to a multi-sensor array to realize real-time and high spatial resolution monitoring of dynamic deformations across the entire cortex (Figure 5; Figure S13, Supporting Information). More complex dynamic mechanisms of the brain may then be revealed in medium- and large-sized animals, which will facilitate disease monitoring, diagnosis, and treatment.

Supporting Information

Supporting Information is available from the Wiley Online Library or from the author.

Acknowledgements

Z.L. and C.T. contributed equally to this work. This work was supported by the MOST (2022YFA1203001, 2022YFA1203002), the NSFC (52122310, 22075050, T2321003, 22335003), the STCSM (21511104900, 20JC1414902).

Conflict of Interest

The authors declare no conflict of interest.

Data Availability Statement

The data that support the findings of this study are available in the supplementary material of this article.

Keywords

brain deformation, capacitive sensor, implantable electronics

Received: November 6, 2023
Revised: December 21, 2023
Published online: January 12, 2024

[1] L. Galvani, *De Bonoiensi Scientiarum et Artium Intituo atque Academie Commentarii* 1791, 7, 363.

- [2] G. Hong, C. M. Lieber, *Nat. Rev. Neurosci.* **2019**, *20*, 330.
- [3] R. N. Adams, *Anal. Chem.* **1976**, *48*, 1126A.
- [4] J. Li, Y. Liu, L. Yuan, B. Zhang, E. S. Bishop, K. Wang, J. Tang, Y.-Q. Zheng, W. Xu, S. Niu, L. Beker, T. L. Li, G. Chen, M. Diyaolu, A.-L. Thomas, V. Mottini, J. B.-H. Tok, J. C. Y. Dunn, B. Cui, S. P. Pasca, Y. Cui, A. Habtezion, X. Chen, Z. Bao, *Nature* **2022**, *606*, 94.
- [5] J. Livet, T. A. Weissman, H. Kang, R. W. Draft, J. Lu, R. A. Bennis, J. R. Sanes, J. W. Lichtman, *Nature* **2007**, *450*, 56.
- [6] a) G. J. Kress, N. Yamawaki, D. L. Wokosin, I. R. Wickersham, G. M. G. Shepherd, D. J. Surmeier, *Nat. Neurosci.* **2013**, *16*, 665; b) B. J. Hunnicutt, B. R. Long, D. Kusefoglou, K. J. Gertz, H. Zhong, T. Mao, *Nat. Neurosci.* **2014**, *17*, 1276.
- [7] J. Kim, B. Avants, S. Patel, J. Whyte, B. H. Coslett, J. Pluta, J. A. Detre, J. C. Gee, *Neuroimage* **2008**, *39*, 1014.
- [8] S. Bauer, C. May, D. Dionysiou, G. Stamatakos, P. Buchler, M. Reyes, *IEEE Trans. Biomed. Eng.* **2012**, *59*, 25.
- [9] J. J. Sloots, G. J. Biessels, J. J. M. Zwanenburg, *Neuroimage* **2020**, *210*, 116581.
- [10] a) S. P. Lacour, G. Courtine, J. Guck, *Nat. Rev. Mater.* **2016**, *1*, 16063; b) R. Feiner, T. Dvir, *Nat. Rev. Mater.* **2018**, *3*, 17076.
- [11] P. Aljabar, K. K. Bhatia, M. Murgasova, J. V. Hajnal, J. P. Boardman, L. Srinivasan, M. A. Rutherford, L. E. Dyet, A. D. Edwards, D. Rueckert, *Neuroimage* **2008**, *39*, 348.
- [12] S. S. Keller, N. Roberts, *Epilepsia* **2008**, *49*, 741.
- [13] S.-L. Jui, S. Zhang, W. Xiong, F. Yu, M. Fu, D. Wang, A. E. Hassanien, K. Xiao, *IEEE Intell. Syst.* **2016**, *31*, 66.
- [14] a) H. Iida, H. Ohata, M. Iida, Y. Watanabe, S. Dohi, *Anesthesiology* **1998**, *89*, 954; b) B. F. Matta, K. J. Heath, K. Tipping, A. C. Summors, *Anesthesiology* **1999**, *91*, 677.
- [15] K. Yamagishi, I. Kirino, I. Takahashi, H. Amano, S. Takeoka, Y. Morimoto, T. Fujie, *Nat. Biomed. Eng.* **2019**, *3*, 27.
- [16] J. Goeller, A. Wardlaw, D. Treichler, J. O'Bruba, G. Weiss, *J. Neurotrauma* **2012**, *29*, 1970.
- [17] B. M. Basol, V. K. Kapur, C. R. Leidholm, A. Halani, K. Gledhill, *Sol. Energy Mater. Sol. Cells* **1996**, *43*, 93.
- [18] J. Blumm, A. Lindemann, M. Meyer, C. Strasser, *Int. J. Thermophys.* **2010**, *31*, 1919.
- [19] A. Tsukamoto, K. Serizawa, R. Sato, J. Yamazaki, T. Inomata, *Exp. Anim.* **2015**, *64*, 57.
- [20] K. Kato, J. Wakai, K. Ozawa, M. Sekiguchi, K. Katahira, *Exp. Anim.* **2016**, *65*, 393.
- [21] C.-X. Li, S. Patel, D. J. J. Wang, X. Zhang, *Magn. Reson. Imaging* **2014**, *32*, 956.